APS physics

CHORUS

This is the accepted manuscript made available via CHORUS. The article has been published as:

Spin-Ice State of the Quantum Heisenberg Antiferromagnet on the Pyrochlore Lattice

Yuan Huang, Kun Chen, Youjin Deng, Nikolay Prokof'ev, and Boris Svistunov

Phys. Rev. Lett. **116**, 177203 — Published 28 April 2016

DOI: 10.1103/PhysRevLett.116.177203

Spin-Ice State of the Quantum Heisenberg Antiferromagnet on the Pyrochlore Lattice

Yuan Huang[1,2], Kun Chen[1,2],* Youjin Deng[1,2],† Nikolay Prokof'ev[2,3], and Boris Svistunov[2,3]
[1] *National Laboratory for Physical Sciences at Microscale and Department of Modern Physics, University of Science and Technology of China, Hefei, Anhui 230026, China*
[2] *Department of Physics, University of Massachusetts, Amherst, Massahusetts 01003, USA and*
[3] *National Research Center "Kurchatov Institute", 123182 Moscow, Russia*
(Dated: February 29, 2016)

We study the low-temperature physics of the SU(2)-symmetric spin-1/2 Heisenberg antiferromagnet on a pyrochlore lattice and find a "fingerprint" evidence for the thermal spin-ice state in this frustrated quantum magnet. Our conclusions are based on the results of bold diagrammatic Monte Carlo simulations, with good convergence of the skeleton series down to temperature $T/J = 1/6$. The identification of the spin-ice state is done through a remarkably accurate microscopic correspondence for static structure factor between the quantum Heisenberg and classical Heisenberg/Ising models at all accessible temperatures, and the characteristic bow-tie pattern with pinch points observed at $T/J = 1/6$. The dynamic structure factor at real frequencies (obtained by analytic continuation of numerical data) is consistent with diffusive spinon dynamics at pinch points.

PACS numbers: 75.10.Jm, 75.10.Kt, 02.70.Ss

A characteristic feature of all frustrated magnets is close competition among numerous classical spin configurations and absence of an obvious arrangement that gains the maximum amount of energy from all interaction terms [1]. Frustration prevents the development of long-range magnetic orders and often leads to novel and exotic collective phenomena. One of the best known examples is the spin-liquid groundstate [2] that does not break any symmetry and supports fractional elementary excitations and emergent gauge fields.

In many quantum antiferromagnets (AFM), frustration has a simple geometric origin when nearest neighbor (n.n.) spins form triangular or tetrahedral units. The canonical three-dimensional example of such a system is the Heisenberg AFM on a pyrochlore lattice that consists of corner-sharing tetrahedrons. The pyrochlore structure is found in numerous magnetic materials and is directly associated with such exotic low-temperature phenomena as spin glass freezing in $Y_2Mo_2O_7$ and $Y_2Mn_2O_7$ [3–5], classical spin-ice behavior in $Dy_2Ti_2O_7$ and $Ho_2Ti_2O_7$ [6–8], and cooperative paramagnetism down to ultra-low temperatures in $Tb_2Ti_2O_7$ (and, presumably, a spin-liquid groundstate) [9–11].

In this Letter, we study the SU(2)-symmetric spin-1/2 Heisenberg AFM on a pyrochlore lattice,

$$H = J \sum_{<ij>} \boldsymbol{S}_i \cdot \boldsymbol{S}_j \qquad (J > 0)\,, \qquad (1)$$

where $\boldsymbol{S}_i$ is the spin operator on site i, and $\langle \ldots \rangle$ stands for n.n. sites. Despite its simplicity, this model is known to be notoriously difficult to solve at low, but finite, temperature $T < J$ where perturbative treatments are not reliable, conventional Monte Carlo methods suffer from the notorious sign problem (because of frustration), and variational methods are not applicable. As far as we know, diagrammatic Monte Carlo (DiagMC) is the only generic method capable of establishing controlled results in this strongly correlated regime [12–14], which is also the region most frequently studied experimentally.

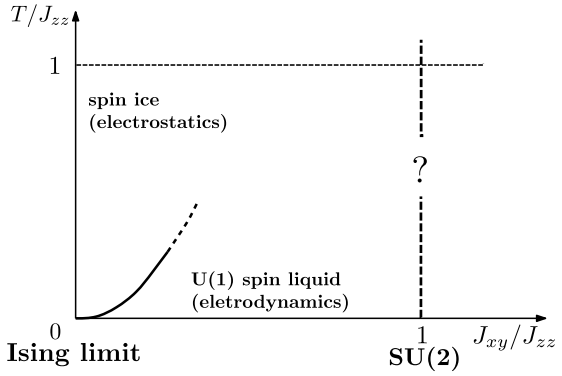

FIG. 1. Sketch of the finite-temperature phase diagram for the XXZ model based on the perturbation theory. For $J_{xy} \ll J_{zz}$, the first crossover at $T \sim J_{zz}$ (dotted line) is to the thermal spin-ice state; it is followed by a second crossover at $T \sim J_{xy}^3/J_{zz}^2$ to the low-temperature U(1) spin-liquid ground state. Whether the spin-ice state survives on approach to the isotropic Heisenberg point, $J_{xy}/J_{zz} = 1$ is beyond the perturbation theory.

Several analytic and numeric studies [16–22] looked at properties of the related XXZ model $H_{\rm XXZ} = \sum_{<ij>} J_{zz} S_i^z S_j^z + J_{xy}(S_i^x S_j^x + S_i^y S_j^y)$ that has lower $U(1) \otimes Z_2$ symmetry, admits perturbative treatment when $J_{xy} \ll J_{zz}$, and reduces to the Ising system at $J_{xy} = 0$. At temperature $T < J_{zz}$, the Ising system features emergent gapped $S_z = 1/2$ spinons that carry fractionalized "electric" charges and interact by Coulomb forces; they remain deconfined because of screening. Charged excitations "freeze out" at low temperature, leaving a massively degenerate ground state manifold. It is known as the spin-ice phase where degenerate states

satisfy the "2-in/2-out" ice rule on each tetrahedron [23] and give rise to dipolar correlations. Its characteristic feature is the bow-tie pattern with pinch point singularities in the static structure factor. Spin-ice states were also predicted to exist in the large-S and large-N limits of spin models [16, 19, 20, 22, 24].

Weak transverse terms, $|J_{xy}| \ll J_{zz}$, can be dealt with by degenerate perturbation theory [18]. At third-order (and low-enough temperature), quantum exchange processes $\propto J_{xy}^3/J_{zz}^2$ operating within the hexagons are argued to lead to the effective "quantum electrodynamics" type system in the continuum limit. In addition to spinons, the system features emergent gapped monopoles carrying fractionalized "magnetic" charges and gapless U(1) gauge bosons, or "photons" [18, 25–27]. The resulting finite temperature phase diagram is illustrated in Fig. 1. The ground state is argued to be a U(1) quantum spin liquid with gapless "photon" excitations. Quantum fluctuations suppress the characteristic pinch-point singularities of the classical spin-ice, and this fact can be used for experimental identification of the spin-liquid state from the structure factor.

To answer what happens in the non-perturbative case, $J_{xy}/J_{zz} \sim 1$, is a far more difficult task. In this Letter, we employ the DiagMC method to study the isotropic case $J_{xy}/J_{zz} = 1$ in (1). We find the spin-ice state dominating system properties over a wide temperature interval, from $T \sim J$ down to the lowest simulated temperature $T = J/6$. At $T = J/6$ the static structure factor features a characteristic bow-tie pattern with pinch points. The ultimate "fingerprint" evidence follows from remarkable quantum-to-classical correspondence (QCC) [13] between the static spin correlation functions of quantum Heisenberg, classical Heisenberg, and classical Ising models on the same lattice at all length scales and all accessible temperatures. Using analytic continuation methods, we compute the dynamic structure factor at real frequencies and observe diffusive spinon dynamics at the pinch points and local spin-fluctuation continuum along the nodal lines. These results are consistent with the effective hydrodynamic theory for the spin ice [20, 28]. A quantum spin-liquid state, if any, may emerge only at temperatures significantly below $J/6$.

DiagMC and Fermionization. The DiagMC is a controlled numerical approach based on stochastic sampling of all skeleton Feynman diagrams up to some high order N and extrapolation to the $N \to \infty$ limit; the series are supposed to be convergent or subject to the analytic continuation beyond convergence radius by resummation protocols [12, 29]. Our implementation of DiagMC for (1) is based on the G^2W skeleton expansion in the real-space–imaginary-time representation similar to that described in Refs. [13]. To arrive at the diagrammatic formulation, spins in Eq. (1) are replaced with localized fermions: $\boldsymbol{S}_i = \frac{1}{2}\sum_{\alpha\beta} f_{i\alpha}^\dagger \boldsymbol{\sigma}_{\alpha\beta} f_{i\beta}$, where $f_{i\beta}$ is the standard fermionic annihilation operator on site i, and $\boldsymbol{\sigma}$ are Pauli matrixes. Since this procedure enlarges the Hilbert space by introducing unphysical states with zero and double fermion occupancy, the Popov-Fedotov trick [14, 15] is to add a complex chemical potential term to (1) to ensure exact cancelation of all unphysical contributions in grand-canonical statistical averages. As a result, one ends up with the interacting flat-band fermionic Hamiltonian

$$H = \frac{J}{4}\sum_{\substack{<ij>\\ \alpha\beta\gamma\delta}} \boldsymbol{\sigma}_{\alpha\beta}\cdot\boldsymbol{\sigma}_{\gamma\delta} f_{i\alpha}^\dagger f_{i\beta} f_{i\gamma}^\dagger f_{i\delta} - \frac{i\pi T}{2}\sum_i (n_i - 1), \quad (2)$$

where $n_i = \sum_\alpha f_{i\alpha}^\dagger f_{i\alpha}$. The DiagMC method is used to sample both the auxiliary single-particle propagators and the physical spin correlation functions. The technique allows us to go far beyond the mean-field approximation and account for all skeleton diagrams up to the 6-th order ($> 10^5$ graphs). We simulate finite systems with periodic boundary conditions and always consider system sizes much larger than the spin correlation length to ensure that finite-size corrections remain negligible.

Correlation function. Magnetic properties are deduced from the correlation function $\chi(\boldsymbol{r}_i, \boldsymbol{r}_j; \tau) = \langle \hat{\boldsymbol{S}}(\boldsymbol{r}_i, 0) \cdot \hat{\boldsymbol{S}}(\boldsymbol{r}_j, \tau)\rangle$, where $\boldsymbol{r}_i$ is the radius vector of the lattice site i. The structure factor in the momentum–Matsubara-frequency domain is given by $S(\boldsymbol{Q}, i\omega_n) = (1/V)\sum_{i,j}\int_0^\beta d\tau \chi(\boldsymbol{r}_i, \boldsymbol{r}_j; \tau) e^{-i[\boldsymbol{Q}\cdot(\boldsymbol{r}_j - \boldsymbol{r}_i) + \omega_n \tau]}$ where $\boldsymbol{Q}$ belongs to the first Brillouin zone (BZ), $\omega_n = 2\pi n/\beta$ is the Matsubara frequency, and V is total number of spins. Static response is described by $S(\boldsymbol{Q}, 0)$, and the uniform magnetic susceptibility χ_u is given by $S(0, 0)$.

In Fig. 2 we compare DiagMC and the high-temperature expansion [30] results for χ_u. At high temperature $T/J > 2$ the agreement between the two methods is at the level of three meaningful digits. As temperature is lowered below $1.5J$, the high-T series explode while the diagrammatic series continue to converge at least down to $T/J \approx 1/6$. In the inset of Fig. 2 we show how χ_u depends on the inverse diagram order $1/N$ at $T/J = 1/2$. This temperature is well below the divergence point of the high-T series and, thus, is in the strongly correlated paramagnetic regime. Clearly, the answer does not change outside of error bars after accounting for 5-th and 6-th order diagrams.

In Fig. 3, we show the evolution of the static structure factor in the $([hh0][00l])$ plane of the reciprocal space from high ($T/J = 2$) to low ($T/J = 1/6$) temperature. As the temperature is lowered, the system goes through a smooth crossover from the high-T state with the checkerboard pattern in $S(\boldsymbol{Q}, 0)$ to the low-T state with the bow-tie pattern and pseudo-singular pinch points. As pointed out in Refs. [19, 20], these strongly anisotropic pinch points are a direct consequence of the "2-in/2-out" ice rule. All by itself, this is strong evidence that at $T/J = 1/6$ the isotropic Heisenberg model is dominated

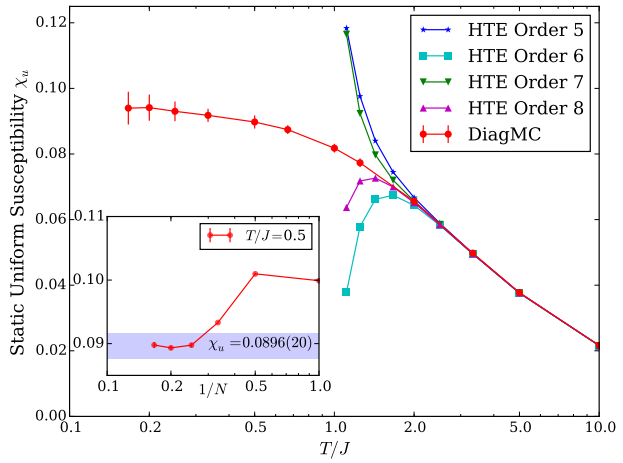

FIG. 2. (Color online) Uniform susceptibility χ_u as a function of temperature from the DiagMC approach(red circles) and from the high temperature expansion (HTE) method [30] truncated at different expansion orders. Inset: χ_u at $T/J = 1/2$ as a function of inverse maximal skeleton diagram order N. The errorbar on the final answer, shown as the blue region, is a combination of statistical Monte Carlo errors for fixed-N points and the systematic error of extrapolation to the $N \to \infty$ limit.

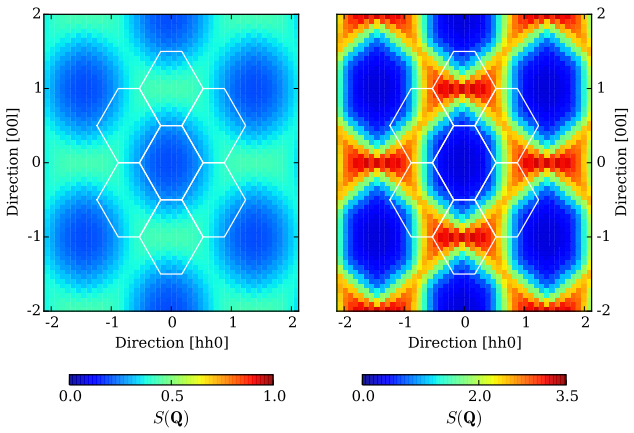

FIG. 3. (Color online) Structure factor $S(\boldsymbol{Q})$ in the $([hh0][00l])$ plane at $T/J = 2$ (left panel) and $T/J = 1/6$ (right panel). Note that the color scheme contrast (shown at the bottom) is significantly enhanced for the left panel.

by the spin-ice physics with excitations forming a dilute gas of "electric" charges.

Quantum-to-classical correspondence. Taking system configuration "snapshots" is equivalent to considering multi-point correlation functions in the diagrammatic approach (an impossible task for a large collection of spins), not to mention that the standard technique calculates their statistical averages. QCC comes to rescue here. In addition to (1), we consider the Ising model with spins $s = \pm 1$ and the classical Heisenberg model with unit-vector spins $\boldsymbol{s}$ on the pyrochlore lattice. Both classical

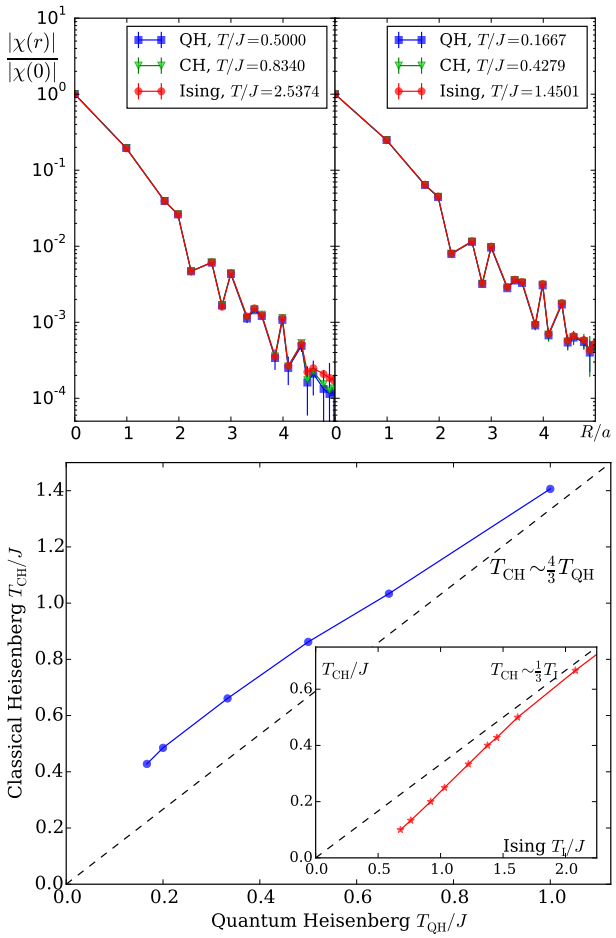

FIG. 4. (Color online) Upper panel: Normalized static susceptibilities (by modulus), $|\chi_s(\boldsymbol{r})/\chi_s(0)|$, in quantum Heisenberg, classical Heisenberg and classical Ising models at temperatures $T_{QH}/J = 1/2$, $T_{CH}/J = 0.8340$, $T_I/J = 2.5374$ (left panel), and $T_{QH}/J = 1/6$, $T_{CH}/J = 0.4279$, $T_I/J = 1.4501$ (right panel). The QCC is satisfied within the error bars at all distances. Lower panel: Quantum-to-classical temperature relationship plot T_{CH} *vs* T_{QH}. The straight black line is the high-T relation $T_{CH} = (4/3)\, T_{QH}$. Inset: temperature relationship T_{CH} *vs* T_I between the classical Heisenberg and Ising systems. The straight black line is the high-T relation $T_{CH} = (1/3)\, T_I$.

models have nearly identical bow-tie patterns in $S(\boldsymbol{Q})$ at $T = 0$ [19, 20]. What we establish here, is an accurate QCC for spin correlation functions (static in the quantum case) between the original quantum model at temperature T_{QH} and its classical counterparts at temperatures T_I and T_{CH}, respectively. The result is the "fingerprint" identification of dominant system configurations at low-T as originating from the spin-ice state (temperatures need to be fine-tuned because quantum and classical models have different spin values and configuration spaces [13]).

The QCC protocol is as follows. For the quantum system, we compute the static correlation function $\chi(\boldsymbol{r}) \equiv \int_0^\beta d\tau \chi(\boldsymbol{r}_0, \boldsymbol{r}_i; \tau)$ where $\boldsymbol{r} = \boldsymbol{r}_i - \boldsymbol{r}_0$ (its classical counter-

parts are defined similarly without the τ-dependence). We normalize the correlation functions to unity at the origin, $f(\boldsymbol{r}) = \chi(\boldsymbol{r})/\chi(0)$, and then consider the classical-model temperature ($T_{\rm I}$ or $T_{\rm CH}$) as a free parameter to obtain the best fit for $f(\boldsymbol{r})$ curves. The essence of QCC is that the entire functional dependence $f(\boldsymbol{r})$ is reproduced with high accuracy at all distances with this minimally required effort [13].

Remarkably, we observe a perfect match between the quantum result at $T_{\rm QH}$ and classical results at rescaled temperatures; the accuracy is at the sub-percent level at any temperature. In Fig. 4(a) we show two examples of QCC at $T_{\rm QH}/J = 1/2$ and $T_{\rm QH}/J = 1/6$. Since system "snapshots" are readily available in classical models, the identification of the quantum state becomes unambiguous. [It should be noted that QCC is absent for the equal-time correlation function $\chi(\boldsymbol{r}, \tau = 0)$.] The relationship between the temperature of the quantum Heisenberg model and its classical counterpart is plotted in the lower panel of Fig. 4; the relationship between the classical temperatures is shown in the inset of the lower panel in Fig. 4.

It is not surprising to observe QCC in two limiting cases: (i) at high temperature $T/J \gg 1$ when weak short-range correlations are captured at the lowest series-expansion order, and (ii) at distances much larger than the correlation length where statistical description in terms of the coarse-grained field becomes universal. What we observe is different: the correspondence holds at all distances starting from the nearest-neighbor sites and at all temperatures, including the crossover region $T/J \sim 1$. Similarly accurate QCC was reported for Heisenberg models on the square and triangular lattices [13] (it fails in 1D). Currently, sharp theoretical understanding of QCC for spin-1/2 magnetic systems in $D > 1$ is missing.

Having established that static properties correspond to those of the spin ice, we proceed with the study of dynamic response and compute the structure factor on the real frequency axis. This quantity can be directly measured in inelastic neutron scattering experiments. Real and Matsubara frequency functions are related to each other by the standard linear-response theory relation

$$S(\boldsymbol{Q}, i\omega_n) = \frac{1}{\pi}\int_0^\infty \frac{(1-e^{-\beta\omega})\omega}{\omega_n^2+\omega^2} S(\boldsymbol{Q}.\omega)d\omega \qquad (3)$$

This integral equation is solved using numerical analytic continuation methods [31, 32]. The result for two characteristic momentum points $\boldsymbol{Q}_1 = (0, 0, \frac{2\pi}{a})$ and $\boldsymbol{Q}_2 = (0, 0, \frac{5\pi}{4a})$, where a is the lattice constant, is shown in Fig. 5. On the basis of the thermal spin-ice picture, we expect two dynamic contributions: one from slow diffusive motion of spinons and the other from propagating spin waves. At the pinch point $\boldsymbol{Q}_1$, the dynamic response is best described as that of the diffusive (Drude-type) spinon peak [20, 28] . The second point $(0, 0, \frac{5\pi}{4a})$ is on one of the nodal lines, which correspond to special directions along which the spinon contribution is suppressed due to the ice rule and lattice structure [20]. Indeed, for this point the diffusive peak at $\omega = 0$ is absent, and a broad continuum originating from local spin fluctuations with the typical energy scale $\omega \sim J$ emerges instead.

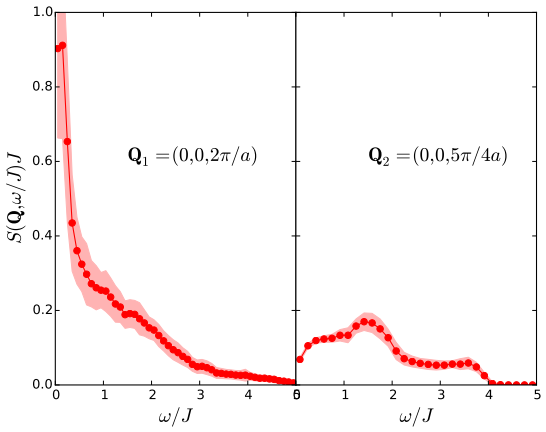

FIG. 5. (Color online) Dynamic structure factor as a function of frequency at the pinch point $\boldsymbol{Q}_1 = (0, 0, 2\pi/a)$ (left panel) and on the nodal line at $\boldsymbol{Q}_2 = (0, 0, 5\pi/4a)$.

Discussion. Using the DiagMC technique, we carried out a systematic investigation of the quantum SU(2)-symmetric Heisenberg AFM on the pyrochlore lattice. The correlated paramagnetic state at temperature well below the exchange coupling constant is unambiguously identified as the thermal spin-ice phase. The U(1) spin liquid (predicted from perturbative studies of the strongly anisotropic XXZ model) has not been observed. Apparently, the characteristic temperature to see the emergent gauge structure is much lower than $T/J = 1/6$.

Our work paves the road for applications of DiagMC to studies of frustrated magnetic materials with complicated Hamilitonians when in (1) the exchange constant J is replaced with a 3×3 tensor and interactions are extended beyond the nearest-neighbor sites [33, 34]. Dealing with such Hamiltonians does not present any additional burden for the DiagMC method because in the skeleton formulation all lines are automatically assumed to be fully renormalized and non-local in space-time. Our work demonstrates that it is possible to use DiagMC to perform accurate *ab initio* calculations of both static and dynamic response for frustrated magnets, and obtain results that can be directly compared with experiments such as the inelastic neutron scattering. In particular, one's ability to enter the strongly correlated regime and accurately compute properties at temperatures significantly below J leads to the possibility of extracting the relevant Hamiltonian parameters for frustrated magnetic materials from measurements.

Acknowledgements. We thank O. Starykh, G. Chen,

A. Mishchenko, and especially late C. Henley (who corresponded with us while being terminally ill) for advice, technical assistance, and inspiring discussions. This work was supported by the Simons Collaboration on the Many Electron Problem, National Science Foundation under the grant PHY-1314735, the MURI Program "New Quantum Phases of Matter" from AFOSR, CAS, and the National Science Foundation of China (NSFC) under Grant No. 11275185.

* chenkun@mail.ustc.edu.cn
† yjdeng@ustc.edu.cn

[1] A. P. Ramirez, Annu. Rev. Mater. Sci. **24**, 453-480 (1994).
[2] P. W. Anderson, Mater. Res. Bull. **8**, 153 (1973).
[3] J. N. Reimers, J. E. Greedan, R. K. Kremer, E. Gmelin, and M. A. Subramanian, Phys. Rev. B **43**, 3387 (1991).
[4] J. S. Gardner, B. D. Gaulin, S.H. Lee, C. Broholm, N. P. Raju, and J. E. Greedan, Phys. Rev. Lett. **83**, 211 (1999).
[5] C. H. Booth, J. S. Gardner, G. H. Kwei, R. H. Heffner, F. Bridges, and M. A. Subramanian, Phys. Rev. B **62**, R755 (2000).
[6] M. J. Harris, S. T. Bramwell, D. F. McMorrow, T. Zeiske, and K. W. Godfrey, Phys. Rev. Lett. **79**, 2554 (1997).
[7] R. Siddharthan, B. S. Shastry, A. P. Ramirez, A. Hayashi, R. J. Cava, and S. Rosenkranz, Phys. Rev. Lett. **83**, 1854 (1999).
[8] S. T. Bramwell and M. J. P. Gingras, Science **294**, 1495 (2001).
[9] J. S. Gardner, B. D. Gaulin, A. J. Berlinsky, P. Waldron, S. R. Dunsiger, N. P. Raju, and J. E. Greedan, Phys. Rev. B **64**, 224416 (2001).
[10] S. W. Han, J. S. Gardner, and C. H. Booth. Phys. Rev. B **69**, 024416 (2004).
[11] T. Fennell, M. Kenzelmann, B. Roessli, M. K. Haas, and R. J. Cava, Phys. Rev. Lett. **109**, 017201 (2012).
[12] N. V. Prokof'ev and B. V. Svistunov, Phys. Rev. Lett. **99**, 250201 (2007).
[13] S. A. Kulagin, N. V. Prokof'ev, O. A. Starykh, B. V. Svistunov, and C. N. Varney, Phys. Rev. Lett. **110**, 070601 (2013); *ibid.* Phys. Rev. B **87**, 024407 (2013).
[14] N. V. Prokof'ev and B. V. Svistunov, Phys. Rev. B **84**, 073102 (2011).
[15] V. N. Popov and S. A. Fedotov, Sov. Phys. JETP **67**, 535 (1988); Proc. Steklov Inst. Math. **177**, 184 (1991).
[16] R. Moessner and J. T. Chalker, Phys. Rev. Lett., **80**, 2929 (1998); R. Moessner and J. T. Chalker, Phys. Rev. B., **58**, 12049 (1998).
[17] B. Canals, and C. Lacroix, Phys. Rev. Lett., **80**, 2933 (1998); B.Canals, and C. Lacroix, Phys. Rev. B, **61**, 1149 (2000).
[18] M. Hermele, M. P. A. Fisher, and L. Balents, Phys. Rev. B **69**, 064404 (2004).
[19] S. V. Isakov, K. Gregor, R. Moessner, and S. L. Sondhi, Phys. Rev. Lett. **93**, 167204 (2004).
[20] C. L. Henley, Phys. Rev. B **71**, 014424 (2005).
[21] R. Moessner, and A. P. Ramirez, Phys. Today, **59(2)**, 24 (2006).
[22] C. L. Henley, Annu. Rev. Condens. Matter Phys. **10**.1146 (2010).
[23] Anderson PW, Phys. Rev. **102**, 1008 (1956)
[24] M. P. Zinkin, M. J. Harris, T. Zeiske, Phys. Rev. B **56**, 11786 (1997).
[25] M. J. P. Gingras and P. A. McClarty, Rep. Prog. Phys. **77**, 056501 (2014).
[26] A. Banerjee, S. V. Isakov, K. Damle, and Y. B. Kim, Phys. Rev. Lett. **100**, 047208 (2008).
[27] J. P. Lv, G. Chen, Y. Deng, and Z. Y. Meng Phys. Rev. Lett. **115**, 037202 (2015).
[28] P. H. Conlon and J. T. Chalker, Phys. Rev. Lett. 102, 237206 (2009).
[29] K. Van Houcke, F. Werner, E. Kozik, N. V. Prokof'ev, B. V. Svistunov, M. J. H. Ku, A. T. Sommer, L. W. Cheuk, A. Schirotzek, and M. W. Zwierlein, Nat. Phys. **8**, 366370 (2012).
[30] H. J. Schmidt, A. Lohmann, and J. Richter, Phys. Rev. **B 84**, 104443 (2011).
[31] A. S. Mishchenko, N. V. Prokof'ev, A. Sakamoto, and B. V. Svistunov, Phys. Rev. B **62**, 6317 (2000); A. S. Mishchenko, in *Correlated Electrons: From Models to Materials*, eds. E. Pavarini, W. Koch, F. Anders, and M. Jarrell, Forschungszentrum Julich GmbH, (2012).
[32] N. V. Prokof'ev and B. V. Svistunov, JETP Lett. **97**, 649 (2013).
[33] K. A. Ross, L. Savary, B. D. Gaulin, and L. Balents Phys. Rev. X **1**, 021002 (2011).
[34] S. H. Curnoe, Phys. Rev. B **78**, 094418 (2008).